A Physics-Based Analytical Formulation for the Tunneling Current through the Base of Bipolar Transistors Operating at Cryogenic Temperatures

Michael Schröter, Senior Member IEEE, and Xiaodi Jin

Abstract - A physics-based analytical solution for the direct tunneling current through the base region of bipolar transistors operating at cryogenic temperatures is derived. The obtained formulation is continuously differentiable over the entire bias region and contains only few experimentally determinable model parameters, which makes it well-suited for compact circuit modeling. Very good agreement of the new formulation with both a numerical evaluation of the tunneling current integral and experimental data of two SiGe HBT process generations is demonstrated.

Index Terms - bipolar transistor, HBT, cryogenic operation, tunneling current, low-temperature electronics.

I. Introduction

For many years, radio astronomy and space communications have mainly driven the applications at cryogenic temperatures (i.e. up to 93 K). Most recently though, various attempts of building quantum computers have led to a strong interest in using semiconductor technologies at cryogenic temperatures. Depending on the qubit representation, electronic circuits (e.g., for readout) are expected to operate in the range of 0.1 K to about 4 K [1, 2]. In addition, large-scale quantum computing requires a large number of circuits to be integrated on a single chip [1-4]. This makes CMOS and Silicon-Germanium (SiGe) heterojunction bipolar transistor (HBT) process technologies very attractive compared to more exotic technologies such as high electron mobility transistors. At cryogenic temperatures, SiGe HBTs have been demonstrated to possess excellent performance (e.g. [5-9]), including high current gain and speed, which can be traded for low noise and low power consumption [4, 6, 9, 10-12].

Designing integrated circuits requires, among others, compact models for the various devices. So far, HBT compact models for cryogenic applications have been based on physical effects and associated model formulations that are valid at room temperature (RT). For low-temperature circuit design, the model parameters are then adjusted in an attempt to capture the transistor behavior at a particular cryogenic temperature (CT) and a selected bias point (e.g. [4, 6, 13, 14]). Other

Affiliation:

¹Chair for Electron Devices and Integrated Circuits, TU Dresden, Germany.

approaches attempt to expand certain model parameters of existing compact model formulations by temperature dependent polynomials or other non-physical fit functions for capturing the electrical characteristics over bias and a lowtemperature range (e.g. [15-17]). However, carrier transport mechanisms at CT differ from those at RT, making it difficult or even impossible to describe the bias dependent large-signal behavior measured at CT. Fig. 1 demonstrates this problem for the example of the collector current, which is one of the most important components for circuit design since it determines the transconductance of the transistor and the circuit gain. For both technology generations shown in Fig. 1, the drift-diffusion (DD) formulation, on which all present compact models are based on, remains the dominant component down to about 73 K. However, below that temperature DD transport quickly fades away and does not enable an approximation of the measured data anymore. E.g., in Fig. 1(a), the DD current is not even visible at 23 K and below. At these temperatures, direct tunneling from emitter to collector becomes the dominant component for the transfer (and thus static collector) current in advanced HBTs [18-20, 8]. The base current in Fig. 1 just indicates the lower limit of the current gain at very low injection.

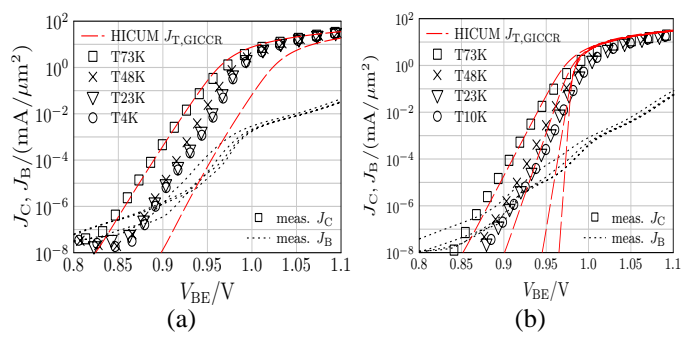


Fig. 1. Collector current density versus base-emitter voltage for low temperatures and two different SiGe HBT process technology generations (a) SG13G2 [21] and (b) a DOTSEVEN [22] variant, both from IHP, Frankfurt/Oder, Germany. Comparison of measured data (symbols) with simulated drift-diffusion current density (dashed lines).

Presently, an HBT compact model that contains physics-based formulations for the effects occurring at CT does not exist. For instance, the transfer tunneling current has been investigated in detail in [18, 19, 20] based on numerical device simulation, which is not suitable though for circuit design. In [18], the tunneling current is calculated from an analytical approximation with a numerical evaluation of an integral over the square of the spatially dependent barrier potential. The latter was obtained from device simulation. Besides being computationally expensive, the formulation becomes discontinuous

when the barrier disappears, making it unsuitable for use in compact models. In comparison, this work presents the first physics-based compact analytical and computationally efficient formulation describing the direct tunneling current through the base region at CT as a function of bias, temperature, barrier height and width with model parameters that can be determined from measurements.

Section II discusses the base barrier profile in SiGe HBTs. Section III contains the derivation of the transmission factor, which is then used in section IV for deriving the current expression. The analytical result is compared in section V to a numerical evaluation of the underlying current integral and then in section VI to experimental data. All considerations assume npn transistors but can be easily applied to pnp transistors.

II. BARRIER PROFILE IN A SIGE HBT BASE REGION

Fig. 2(a) shows the conduction band in vertical (x) direction of the HBT structure at $T=30~\mathrm{K}^1$ for different internal base-emitter (BE) voltages $V_{\mathrm{B'E'}}$ and a collector-emitter voltage $V_{\mathrm{C'E'}}=0.5~\mathrm{V}$. Relative to the conduction band level $W_{\mathrm{C,E}}$ in the emitter, the potential energy profile in the base region poses a barrier for electron injection into the base and constituting the transfer current density J_{T} . Thus, at low temperatures J_{T} is dominated by direct tunneling of electrons from the emitter to the collector.

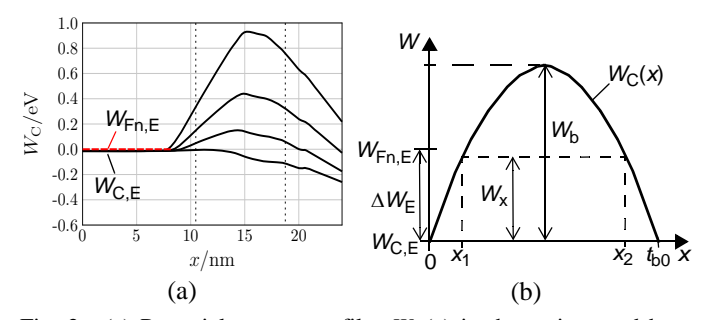


Fig. 2. (a) Potential energy profiles $W_{\rm C}(x)$ in the emitter and base region along the vertical direction x obtained from numerical device simulation² at T=30 K for $V_{\rm B'E'}/V=0$, 0.5, 0.8, 1 and $V_{\rm C'E'}=0.5$ V; vertical dotted lines indicate the BE and BC junction. (b) Schematic of parabolic (potential) energy profile in the base region assumed for analytical treatment and definition of relevant variables.

For deriving a closed-form expression for the tunneling current, the shape of the barrier is approximated here by a parabolic potential (energy) profile,

$$W_C(x) = W_b \left[1 - \left(\frac{2x}{t_{b0}} - 1 \right)^2 \right]$$
 (1)

as sketched in Fig. 2(b). Here, t_{b0} is the barrier thickness at equilibrium and x_1 and x_2 are the classical tunneling turning points associated with the kinetic energy W_x of carriers with a

wave vector component in x-direction, i.e. vertical to the barrier. Furthermore,

$$W_b = q(V_{DEi} - V_{R'E'}) \tag{2}$$

is the bias dependent barrier height with q as elementary charge, $V_{\rm DEi}$ as the built-in voltage of the internal BE junction.

For the derivation below, all energies are referenced to $W_{\rm C,E}$. Hence, $\Delta W_{\rm E}$ is the difference between the electron Fermi level $W_{\rm Fn,E}$ in the emitter and $W_{\rm C,E}$.

III. TUNNELING TRANSMISSION PROBABILITY

The analytical expression for the transmission probability is derived based on the WKB approximation [24],

$$T_{tu}(W_x) = \sqrt{\frac{k_{x1}}{k_{x2}}} \exp\left(-2\int_{x_1}^{x_2} |k_{xb}(W_x)| dx\right).$$
 (3)

Only carriers with a kinetic energy component in x-direction can enter the barrier, which are represented here by the wave vector k_{xb} in the barrier region. Be W_x the energy level of the carriers in the emitter that are incident on the barrier. Then, with the barrier energy profile $W_C(x)$ and assuming a parabolic W(k) relation, k_{xb} can be related to the energy via

$$W_C(x) - W_x = \frac{\hbar^2 k_{xb}^2}{2m_x} \tag{4}$$

with $m_{\rm x}$ as effective electron mass for carrier transport in x-direction and \hbar as reduced Planck constant. Tunneling occurs only for $W_{\rm x} < W_{\rm C}(x)$, which yields

$$|k_{xb}(x)| = \sqrt{\frac{2m_x(W_C(x) - W_x)}{\hbar^2}}.$$
 (5)

Inserting (5) with (1) into (3) yields

$$\int_{x_1}^{x_2} |k_{xb}| dx = \sqrt{\frac{2m_x}{\hbar^2}} \int_{x_1}^{x_2} \sqrt{W_s - W_b \left(\frac{2x}{t_{b0}} - 1\right)^2} dx$$
 (6)

with $W_s = W_b - W_x$ and

$$x_{1,2} = \frac{t_{b0}}{2} \left(1 \mp \sqrt{1 - \frac{W_x}{W_b}} \right). \tag{7}$$

The closed-form solution of (6) is

$$\int_{x_1}^{x_2} |k_{xb}| dx = t_{b0} \frac{\pi}{4} \sqrt{\frac{2m_x}{\hbar^2}} \frac{W_b - W_x}{\sqrt{W_b}}.$$
 (8)

For calculating the transmission factor (3), the wave vectors k_{x1} and k_{x2} are assumed to be the same, since at the low temperatures considered here scattering related transport is small (vs. tunneling). Inserting (8) into (3) then gives

$$T_{tu}(W_x) = \exp\left(-t_{b0}\frac{\pi}{2}\sqrt{\frac{2m_x}{\hbar^2}}\frac{W_b - W_x}{\sqrt{W_b}}\right). \tag{9}$$

Defining the bias dependent exponent variable

For lower temperatures, it is difficult to achieve convergence in a drift-diffusion simulation program.

^{2.} SiGe HBT roadmap technology generation N5 [23].

$$B = t_{b0} \frac{\pi}{2} \sqrt{\frac{2m_x}{\hbar^2 W_b}} \tag{10}$$

with the unit 1/(VAs) allows a more compact writing for the transmission factor as a function of W_x :

$$T_{tu}(W_x) = \exp(-B(W_b - W_x)). \tag{11}$$

IV. TRANSFER TUNNELING CURRENT FORMULATION

Electrons from occupied energy states in the emitter can tunnel directly into available states in the collector. The corresponding tunneling current in *x*-direction is generally given by [24]

$$J_{Ttu} = \frac{2qM_{v}}{(2\pi)^{3}} \int_{-\infty}^{\infty} \int_{-\infty}^{\infty} \int_{k_{x}=0}^{\infty} T_{tu} f_{nE}(1 - f_{nC}) v_{x} dk_{x} dk_{y} dk_{z}$$
 (12)

with $M_{\rm v}$ as the number of equivalent conduction band valleys and $f_{\rm nE}$ ($f_{\rm nC}$) as Fermi function before (index "E") and after (index "C") the barrier,

$$f_n = \frac{1}{1 + \exp\left(\frac{W - W_{Fn}}{k_B T}\right)}.$$
 (13)

In (12), the lower integral bound in x-direction indicates that only carriers with positive velocity v_x (i.e. $k_x > 0$) contribute to the tunneling process from emitter to collector. Neglecting the carrier energy (i.e. the integration over k_y and k_z) parallel to the BE junction leads to a simplified solution [8]. However, the latter neither captures the correct behavior of the tunneling current once the barrier height drops below the Fermi level nor results in a consistent smooth extension towards thermionic emission at higher injection. Note that quasi-ballistic transport is assumed within $0 \le x \le x_1$; i.e. there is no scattering until the carriers hit the barrier energy profile at x_1 . This assumption is justified due to the small distances and the low temperature considered for the derivation.

As shown in Fig. 2(a), for forward operation (including saturation) the conduction band edge in the collector is always equal to or below the conduction band edge in the emitter. Furthermore, due to the moderate collector doping concentration, the electron Fermi level in the collector is below the conduction band edge so that $f_{\rm nC}$ << 1. The total energy W of a carrier in the (thermalized) emitter consists of a potential component and a kinetic component:

$$W = W_{C,E} + W_{kin} = W_{C,E} + W_x + W_{yz}.$$
(14)

For parabolic bands, the kinetic energy components in the emitter are

$$W_x = \frac{\hbar^2 k_x^2}{2m_x}$$
 and $W_{yz} = \frac{\hbar^2 (k_y^2 + k_z^2)}{2m_{yz}} = \frac{\hbar^2 k_{yz}^2}{2m_{yz}}$. (15)

with m_{yz} as effective electron mass for carrier transport parallel to the barrier. Recognizing the carrier momentum $m_x v_x = \hbar k_x$, the term $v_x dk_x$ in (12) can be replaced by dW_x/\hbar . Furthermore, with k_{yz} from (15), $dk_y dk_z = 2\pi k_{yz} dk_{yz}$, which allows to

reduce the double integration in (12) over k-states in the y-z-plane to a single (circular) integration. Hence, using (15) for replacing k_{yz} by the energy W_{yz} , (12) becomes

$$J_{Ttu} = c_T \int_0^\infty \int_0^{W_b} T_{tu}(W_x) f_n(W, W_{Fn}) dW_x dW_{yz}, \qquad (16)$$

with the constant

$$c_T = \frac{2qM_v m_{yz}}{\hbar^3 (2\pi)^2}.$$
 (17)

The lower limit of the integration over W_x reflects the fact that there are no occupied states available below $W_{C,E}$ and that only carriers moving in $+k_x$ direction are of interest. Unfortunately, (16) with (11) does not have a closed-form solution. Therefore, simplifications need to be made for evaluating the integral, which are discussed next.

The energy dependence of the integrand in (16) is shown in Fig. 3 for different bias values $V_{\rm B'E'}$ and setting $W_{\rm Fn}=W_{\rm FN,E}$; i.e. assuming the same carrier distribution at x_1 as in the emitter. At 4 K the Fermi function is very steep around the Fermi level (Fig. 3(a)). Thus the integrand $T_{\rm Tu}f_{\rm n}$ equals just $T_{\rm Tu}$ for energies below the Fermi level. In other words, only energy states within $\Delta W_{\rm E}$ in the emitter contribute to tunneling, so that one can set $f_{\rm n}=1$ and the upper integration limit for the total kinetic energy is given by $\Delta W_{\rm E}$, while the upper integration limit for $W_{\rm x}$ is $\min(\Delta W_{\rm E},W_{\rm b})$ - $W_{\rm yz}$. The assumption of a sharp transition of $f_{\rm n}$ becomes less justified towards higher temperatures as shown in Fig. 3(b) for 77 K. However, at that temperature, the drift-diffusion current still dominates versus the tunneling current according to the measurements shown further below.

Based on the considerations above, an analytical expression for the tunneling current (16) can be derived for the two cases of $W_b \ge \Delta W_E$ and $W_b < \Delta W_E$.

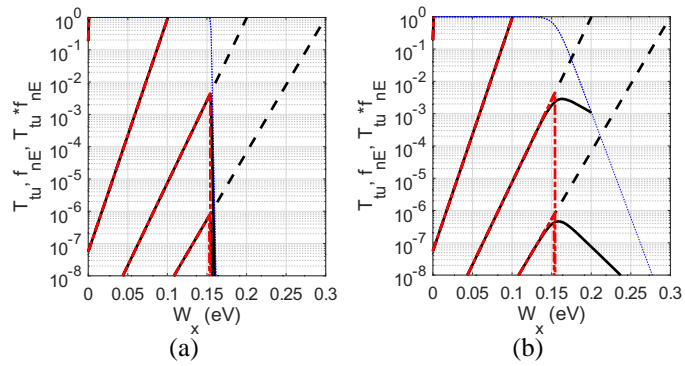


Fig. 3. Tunneling factor (9) (dashed lines), integrand $T_{\rm tu}f_{\rm n}$ (solid lines), Fermi function (dotted line) and $T_{\rm tu}f_{\rm n}(0{\rm K})$ (dashed-dotted line) for (a) 4 K and (b) 77 K, both with $W_{\rm yz}=0$, $\Delta W_{\rm E}=0.155~{\rm eV}$.

A. Barrier height exceeding the Fermi level $(W_b \ge \Delta W_E)$

In this case, (16) can be written as

$$J_{Ttu} = c_T \int_0^{\Delta W_E} \int_0^{\Delta W_E - W_{yz}} T_{tu}(W_x) dW_x dW_{yz}.$$
 (18)

With (11), the inner integral yields

$$\int_{0}^{\Delta W_{E}-W_{yz}} T_{tu} dW_{x} = \frac{\exp(-BW_{b})}{B} [\exp(B(\Delta W_{E}-W_{yz})) - 1]$$
 (19)

and one obtains after performing the integration over $W_{\rm VZ}$

$$J_{Ttu} = \frac{c_T}{B} \Delta W_E \left[\frac{\exp(B \Delta W_E) - 1}{B \Delta W_E} - 1 \right] \exp(-BW_b). \tag{20}$$

Note that *B* is a function of bias.

B.Barrier height below the Fermi level $(W_b < \Delta W_E)$

For this case, two integration intervals have to be considered according to Fig. 4. As long as $0 \le W_{yz} \le \Delta W_E - W_b$, the upper limit for W_x is fixed at W_b . Once W_{yz} exceeds $\Delta W_E - W_b$, the upper limit for W_x depends again on $\Delta W_E - W_{yz}$. Thus, (16) can be rewritten as

$$J_{Ttu} = c_T \left[\int_0^{\Delta W_E - W_b} \int_0^{W_b} T_{tu} dW_x dW_{yz} \right]$$

$$+ \int_{\Delta W_E - W_b}^{\Delta W_E} \int_0^{\Delta W_E - W_{yz}} T_{tu} dW_x dW_{yz}$$
(21)

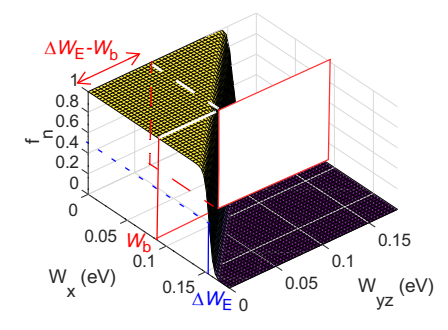


Fig. 4. Fermi function at T = 30 K for illustrating the integration limits in the tunneling current expression once W_b drops below ΔW_E .

Evaluation of the first integral gives

$$\int_{0}^{\Delta W_{E}-W_{b}} \int_{0}^{W_{b}} T_{tu} dW_{x} dW_{yz} = \frac{1-\exp(-BW_{b})}{B} (\Delta W_{E}-W_{b}), (22)$$

while one obtains for the second integral

$$\int_{\Delta W_E - W_b}^{\Delta W_E} \int_0^{\Delta W_E - W_{yz}} T_{tu} dW_x dW_{yz} = \frac{\exp(-BW_b)}{B}$$

$$\left[\frac{\exp(BW_b) - 1}{B} - W_b\right]$$
(23)

Inserting above expressions into (21) yields

$$J_{Ttu} = \frac{c_T}{B} \left[\left[\exp(BW_b) - 1 \right] (\Delta W_E - W_b) + \frac{\exp(BW_b) - 1}{B} - W_b \right] \exp(-BW_b)$$
(24)

In addition to the tunneling current, now also a thermionic current starts flowing for carrier energies larger than W_b . Assuming that the thermionic transmission factor equals one, the thermionic current density is generally given by

$$J_{Tth} = c_T \int_0^\infty \int_{W_h}^\infty f_n(W_x, W_{yz}) dW_x dW_{yz}.$$
 (25)

Unfortunately, the integral over $W_{\rm yz}$ does not have a closed-form solution. Thus, again a zero-K Fermi function is assumed. It leads to

$$J_{Tth} = c_T \int_0^{\Delta W_E - W_b} \int_{W_b}^{\Delta W_E - W_{yz}} dW_x dW_{yz}$$

$$= c_T \frac{(\Delta W_E - W_b)^2}{2}$$
(26)

which is valid for $W_{\rm b} < \Delta W_{\rm E}$ and also is consistent with the tunneling current solution. At very high injection, i.e. once $V_{\rm B^*E^*}$ reaches $V_{\rm DEi}$ and the barrier disappears, the tunneling current drops to zero according to (24) and the thermionic current (26) reaches the value

$$J_{Tth}(W_b \to 0) = J_{TthS} = c_T \frac{\Delta W_E^2}{2}.$$
 (27)

C.Bias dependent barrier width

The device simulations in Fig. 2(a) indicate that not only the barrier height but also the barrier width decreases with $V_{\rm B'E'}$. This does not change the form of the analytical solutions for $J_{\rm Ttu}$ derived so far, but just requires to replace $t_{\rm b0}$ by a bias dependent barrier width

$$t_{b} = t_{b0} \frac{\left(1 - k_{tB} \frac{V_{B'E'}}{V_{DEi}}\right) + \sqrt{\left(1 - k_{tB} \frac{V_{B'E'}}{V_{DEi}}\right)^{2} + 10^{-3}}}{2}$$
(28)

with the model parameter $k_{\rm tB}$ in the range of 0.1...0.2. The simple approximation has been chosen according to device simulation.

V. COMPACT FORMULATION

Below, the previously derived analytical solution is converted to a formulation that is more suitable for compact modeling. First, energies are converted into potentials, leading to

$$V_b = W_b/q = V_{DEi} - V_{B'E'}, (29)$$

$$\Delta V_E = \Delta W_E / q \,. \tag{30}$$

Furthermore, the normalized barrier potential

$$v_b = \frac{V_b}{V_{DEi}} = 1 - \frac{V_{B'E'}}{V_{DEi}}$$
 (31)

and the normalized emitter Fermi potential

$$v_e = \Delta V_E / V_{DEi} \tag{32}$$

are defined. Then, with $c_{\rm T}$ from (17), inserting B from (10) into $c_{\rm T}/B$ in (20) and (24), and extending $\sqrt{W_b}$ by its equilibrium value $\sqrt{qV_{DEi}}$ allows to lump all physical, material and device structure related parameters into the current density prefactor

$$J_{TtuS} = \frac{2qM_v m_{yz}}{h^2 t_{h0} \pi} \sqrt{\frac{2qV_{DEi}}{m_x}} \Delta W_E.$$
 (33)

Defining also the bias independent exponent factor

$$a_{Ttu} = \frac{\pi t_{b0}}{2\hbar} \sqrt{2m_x q V_{DEi}} = B \sqrt{v_b} (q V_{DEi})$$
 (34)

allows writing the exponent arguments

$$BW_b = a_{Ttu} \sqrt{v_b}$$
 and $B\Delta W_E = a_{Ttu} \frac{v_e}{\sqrt{v_b}}$. (35)

Inserting the newly defined factors and normalized barrier potential into (20) yields for $V_b \ge \Delta V_E$ (or $v_b \ge v_e$)

$$J_{Ttu} = J_{TtuS} \sqrt{v_b} \left[\frac{\exp(a_{Ttu}v_e / \sqrt{v_b}) - 1}{a_{Ttu}v_e / \sqrt{v_b}} - 1 \right] \exp(-a_{Ttu} \sqrt{v_b})$$
 (36)

and instead of (24) for $V_b < \Delta V_E$ (or $v_b < v_e$)

$$J_{Ttu} = J_{TtuS} \sqrt{v_b} \left[\exp(a_{Ttu} \sqrt{v_b}) - 1 \right] \left(1 - \frac{v_b}{v_e} \right)$$

$$+ \frac{\exp(a_{Ttu} \sqrt{v_b}) - 1}{a_{Ttu} \sqrt{v_b} / \sqrt{v_b}} - \frac{v_b}{v_e} \right] \exp(-a_{Ttu} \sqrt{v_b})$$
(37)

Moreover, the thermionic current density (26) as a function of (normalized) potentials reads

$$J_{Tth} = J_{TthS} \left(1 - \frac{v_b}{v} \right)^2 \tag{38}$$

with the current density prefactor (27) expressed as

$$J_{TthS} = J_{TtuS} a_{Ttu} \frac{v_e}{2}. (39)$$

The temperature dependence of the derived analytical current density expressions is given by the temperature dependence of the BE built-in voltage [25]

$$V_{DEi}(T) = V_{DEi}(T_0) \frac{T}{T_0} - V_{geff}(0) \left(\frac{T}{T_0} - 1\right) - m_g V_T \ln\left(\frac{T}{T_0}\right)$$
(40)

with T_0 as reference temperature (here 300 K), the model parameter $V_{\rm DEi}(T_0)$ and the fixed parameter

$$m_g = 3 - \frac{k_1}{V_{T0}} = 4.188 \tag{41}$$

with $V_{\rm T0}$ as the thermal voltage at $T_{\rm 0}$. Furthermore, $V_{\rm geff}(0)$ is the effective band gap voltage at 0 K, including high-doping and material composition effects, and $k_{\rm 1}$ is a material dependent constant [26]. Note that (40) is a simplified version of the formulation used in HICUM [25], which is sufficient though at low temperatures.

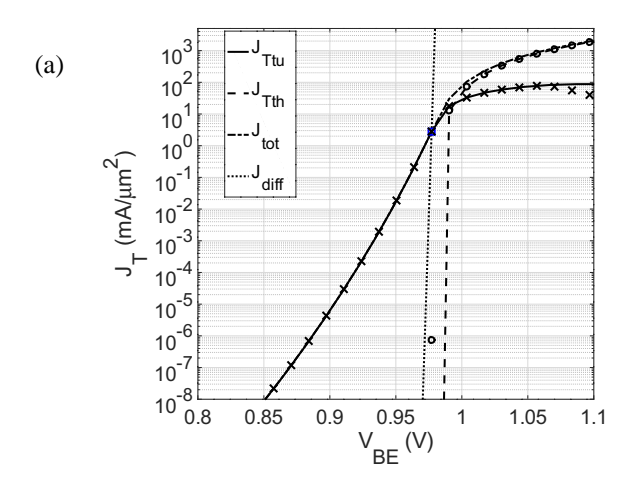
VI. COMPARISON TO NUMERICAL EVALUATION

The analytical results are strictly valid only for the limit T=0 due to the assumption of a step Fermi function. As mentioned earlier, assuming a zero-K Fermi function introduces an error in the current formulation that grows with temperature. For assessing the error, in this section the analytical current formulation is compared to a solution obtained from numerical integration of (16) using the *temperature dependent* Fermi function.

As shown in Fig. 5(a), the solutions (36)-(38) agree very well at 4 K with the numerical evaluation of the current density integrals (16) and (25) when including the temperature dependent Fermi function. The tunneling current increases slightly faster than exponentially for low BE voltages $V_{\rm B'E'}$. Once the barrier height drops below the emitter Fermi level, which happens for $V_{\rm B'E'} > V_{\rm DEi} - \Delta V_{\rm E}$, the tunneling current density increase with $V_{\rm B'E'}$ drops. $J_{\rm Ttu}$ reaches a maximum at high $V_{\rm B'E'}$ and then gradually drops to zero for very high $V_{\rm B'E'}$ when the barrier disappears. However, the total current density,

$$J_{tot} = J_{Ttu} + J_{Tth}, (42)$$

keeps increasing quadratically with $V_{\rm B^*E^*}$ due to the thermionic contribution. Furthermore, the formulations (36)-(38) connect with each other continuously differentiable as displayed in Fig. 5(b) by their derivative, i.e. the transconductance $g_{\rm m}$. Note that $t_{\rm b} = t_{\rm b0}$ was set here.



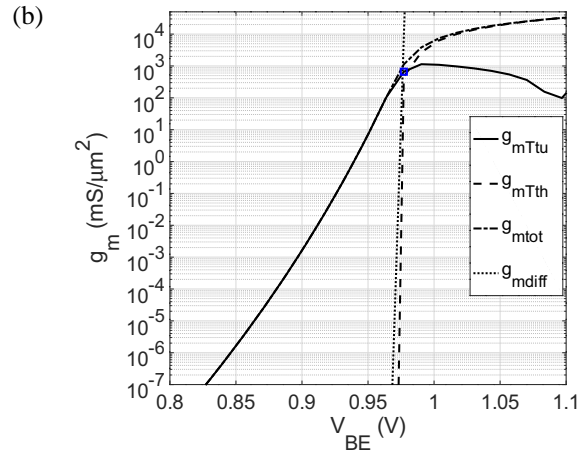


Fig. 5. (a) Tunneling current density (36), (37) (solid lines) and thermionic current density (38) (dashed line) along with the

numerical evaluation of the tunneling current density expression (16) (crosses) and the thermionic current density expression (25) (circles), both including the temperature dependent Fermi function. Also displayed are the analytical total current density (dash-dotted line) and an ideal diffusion current density (dotted line) as reference, all at T = 4 K. (b) Transconductance of the tunneling, thermionic and total current density from the analytical expressions (36)-(38) with the transconductance of an ideal diffusion current as reference (dotted line); T = 4 K.

While the analytical formulation (36)-(38) is still very accurate at 4 K, increasing deviations from the exact solution of (16) and (25) with a T dependent Fermi function are expected towards higher temperatures. These deviations become visible for T=50 K at lower bias and, for $J_{\rm Ttu}$, also at very high bias as shown in Fig. 6. With increasing T, the spread of the Fermi function leads to a larger portion of carriers with higher energies where the tunneling barrier is narrower. These additional contributions are not captured by the analytical expression and result in lower current density values at low injection. The higher energetic carriers also lead to an increase in the thermionic current, which displays the typical DD current slope at low injection in contrast the analytical expression. However, the shape of the bias dependence is still well captured for the total current density over the entire bias range.

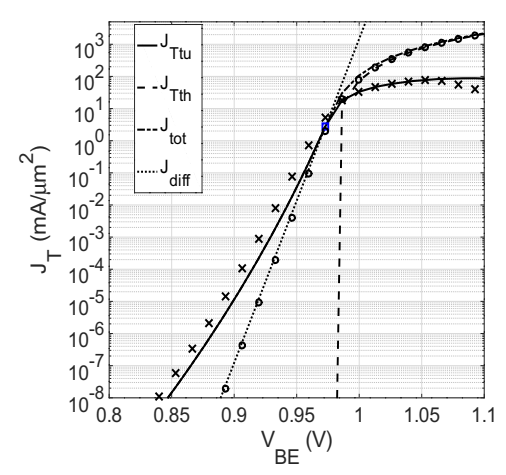


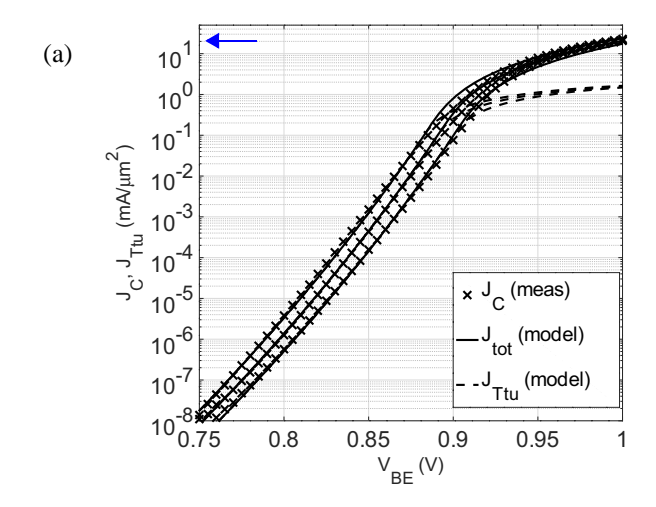
Fig. 6. Tunneling current density (36), (37) (solid lines) and thermionic current density (38) (dashed line) compared with their exact numerical solutions of (16) (crosses) and (25) (circles), all at T = 50 K. Also displayed are the analytical total current density (dash-dotted line) and an ideal diffusion current density (dotted line) as reference.

Finally, setting the transfer current of an HBT equal to $J_{\rm Tth}$ at high injection corresponds to ballistic transport through the base. This may be the case for (future) very advanced transistors [23] but for present production technologies the therminic current expression needs to be extended by carrier scattering in order to be applicable at higher temperatures (above $\approx 70~\rm K$) when the drift-diffusion current dominates the transfer current. In other words, in a compact model, one would either attempt to use the already existing model formulation for the DD transfer current, since it includes the various physical effects occurring also in the collector, or have to

extend the thermionic current expression derived here by scattering effects.

VII. APPLICATION TO EXPERIMENTAL DATA

Fig. 7 shows a comparison of the analytical model (36)-(38) with experimental data from two different process generations. In contrast to the comparison in the previous section, the model parameters J_{TtuS} , a_{Ttu} , ΔV_{E} , $V_{\text{DEi}}(T_0)$ and k_{wB} have to be adjusted to the measured data since neither the barrier width nor the actual barrier profile is known. As the results in Fig. 7 demonstrate, the analytical model allows a quite accurate description of the measured tunneling and thermionic current data over a wide bias and cryogenic temperature range.



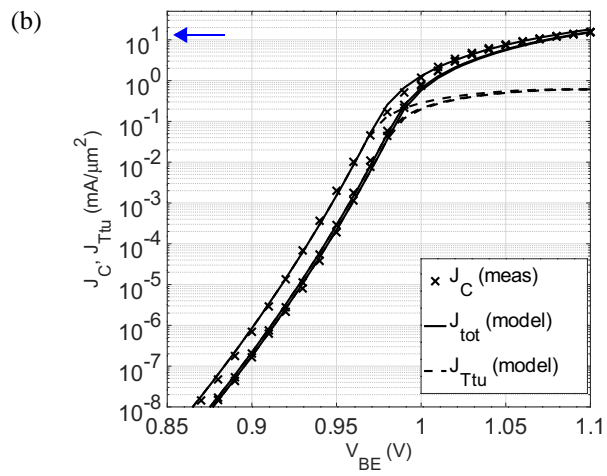


Fig. 7. Collector current density versus terminal BE voltage for different temperatures ($V_{\rm BC}=0$ V). Comparison between analytical model (36)-(38) (lines) with adapted parameters and measured data (symbols) for two different process technologies from IHP: (a) SG13G2 [21] at T/K=4, 48, 63 and (b) a DOTSEVEN process variant at T/K=10, 23, 48 (here, 4 K data were not available). The dashed lines represent the analytical tunneling current only; the arrows indicate $J_{\rm C}(f_{\rm T,peak})$.

The impact of the parameters is as follows. $J_{\rm TtuS}$ shifts the complete curves (consisting of both tunneling and thermionic current contribution) up and down, while $\Delta V_{\rm E}$ shifts the complete curves along the $V_{\rm BE}$ axis. With $a_{\rm Ttu}$ and $k_{\rm wB}$ the bending

of predominantly the tunneling current related curves (i.e. the deviation from the purely exponential behavior) can be adjusted. Furthermore, $V_{\rm DEi}$ determines the spread of the curves for different temperatures. Setting $k_{\rm wB} > 0$ was beneficial only for obtaining the results in Fig. 7(a).

Notice that the parameters for the tunneling current can be extracted independently of whatever suitable DD current formulation is used as long as the DD current is negligible. This is the case at sufficiently low temperatures and sufficiently low bias, where the tunneling current completely dominates. At "intermediate" temperatures, it is difficult to separate the two transport mechanisms. Hence, the DD formulation related parameters need to be extracted at higher temperatures, where DD transport completely dominates. The parameter $V_{\rm DEi}(T_0)$ is usually determined from junction capacitance measurement. If necessary, $V_{\rm DEi}(T_0)$ may be defined separately for the tunneling current formulation to maximize its accuracy. However, this decision depends on the selected compact model.

Device simulation suggests that, for the process technologies investigated here, at temperatures above ≈ 50 K the DD current is not negligible anymore and would have to be included in the comparison. Although the results in Fig. 7 imply that one can use (36)-(38) directly in a compact model, in practice one would have to superimpose the existing DD based formulation in order to describe the collector current characteristics at higher temperatures accurately where the tunneling current becomes negligible. This means that the thermionic current formulation would have to be replaced by the DD formulation of the transfer current. Moreover, the variable v_b defined in (31) would be replaced by a smooth function for avoiding arithmetic overflow at $V_{\rm B'E'} > V_{\rm DEi}$. Finally, $V_{\rm DEi}(T_0)$ may be determined from depletion capacitance measurements [8].

VIII. SUMMARY AND CONCLUSIONS

A compact analytical physics-based formulation for the direct tunneling current through the base region of bipolar transistors has been derived for modeling the transfer current and thus the static collector current at cryogenic temperatures. The new formulation contains the barrier height and width as parameters and covers the entire relevant bias region, including the thermionic current over the barrier at high forward bias. The comparison with experimental data of advanced SiGe HBTs from two process generations shows good agreement of the new formulation over bias and temperature. The implementation in a compact model will require a smoothing function for the bias dependent barrier height, which will enable a reduction of the derived tunneling current formulation to a single equation of the form (24).

Acknowledgments

This work was partially funded by the German National Science Foundation (DFG grant SCHR695/16). The authors are indebted to Dr. B. Heinemann and Dr. H. Rücker, both with IHP Frankfurt/Oder, Germany, for providing hardware and would also like to express their gratitude to N. Weddeler and Dr. P. Sakalas for supporting the initial set-up of the cryogenic

probe station and measurements, and to Markus Müller for parameter extraction support.

References

- [1] L. Vandersypen, "Quantum computing The next challenge in circuit and system design", IEEE ISSCC, pp. 24-29, 2017.
- [2] J. Hsu, "Fast, cold, and under control converntional electronics join quantum circuits in the deep freeze", IEEE Spectrum, p. 10, May 2021.
- [3] J. Bardin, "Analog/mixed-signal integrated circuits for quantum computing", IEEE BiCMOS and Compound Semicond. Integr. Circ. and Technol. Symp. (BCICTS), 8p., 2020.
- [4] J. C. Bardin, "Cryogenic Low-Noise Amplifiers: Noise Performance and Power Dissipation", IEEE Solid-State Circ. Mag., vol. 13, no. 2, pp. 22-35, 2021.
- [5] J. Yuan, J. Cressler, R. Krithivasan, T. Thrivikraman, M. Khater, D. Ahlgren, A. Joseph, J.-S. Rieh, "On the performance limits of cryogenically operated SiGe HBTs and its relation to scaling for THz speeds", IEEE Trans. Electron Dev., vol. 56, no. 5, pp. 1007-1018, 2009.
- [6] N. Waldhoff, F. Danneville, G. Dambrine, B. Geynet, P. Chevalier. "Investigation of SiGe HBT potentialities under cryogenic temperature", IEEE ESSDERC, pp. 121-124, 2009.
- [7] P. S. Chakraborty, A. Cardoso, B. Wier, A. Omprakash, J. Cressler, M. Kaynak, and B. Tillack, "A 0.8 THz SiGe HBT operating at 4.3 K", IEEE Electron Device Lett., vol. 35, no. 2, pp. 151–153, 2014.
- [8] X. Jin, M. Müller, P. Sakalas, A. Mukherjee, Y. Zhang, M. Schröter, "Advanced SiGe:C HBTs at Cryogenic Temperatures and Their Compact Modeling With Temperature Scaling", IEEE J. of Explor. Solid-State Comput. Dev. and Circ., vol. 7, no. 2, pp. 175-183, 2021.
- [9] S. Bonen , G. Cooke , T. Jager , A. Bharadwaj, S. Pati Tripathi , D. Céli, P. Chevalier , P. Schvan, S. P. Voinigescu, "Cryogenic characterization of the high frequency and noise performance of SiGe HBTs from DC to 70 GHz and down to 2 K", IEEE Microw. Wirel. Comp. Lett., vol. 32, no. 6, pp. 696-699, 2022.
- [10] W.-T. Wong, M. Hosseini, H. Rücker, and J.C. Bardin, "A 1 mW cryogenic LNA exploiting optimized SiGe HBTs to achieve an average noise temperature of 3.2 K from 4–8 GHz", IEEE MTT-S Int'l Microw. Symp., pp. 181-184. 2020.
- [11] M. J. Curry, T. England, N. Bishop, G. Ten-Eyck, J. Wendt, T. Pluym, M. Lilly, S. Carr, and M. Carroll, "Cryogenic preamplication of a single electron-transistor using a silicon-germanium heterojunction-bipolar-transistor", Appl. Phys. Lett., vol. 106, no. 20, pp. 203505, 2015.
- [12] S. Montazeri, W.-T. Wong, A. Coskun, J. Bardin, "Ultralow-power cryogenic SiGe low-noise amplifiers: Theory and demonstration", IEEE Trans. Microw. Theory and Techniques, vol. 64, no. 1, pp. 178-187, 2016.
- [13] J. Bardin and S. Weinreb. "Experimental cryogenic modeling and noise of SiGe HBTs", IEEE MTT-S Int'l

- Microw. Symp. Dig., pp. 459-462. 2008.
- [14] H. Ying, S. Rao, J. Teng, M. Frounchi, M. Muller, X. Jin, M. Schröter, J. D. Cressler, "Compact Modeling of SiGe HBTs for Design of Cryogenic Control and Readout Circuits for Quantum Computing", IEEE BiCMOS and Compound Semicond. Integr. Circ. and Technol. Symp. (BCICTS), pp. 17-20, 2020.
- [15] Z. Feng, G. Niu, C. Zhu, L. Najafizadeh, J. Cressler, "Temperature Scalable Modeling of SiGe HBT DC Currents Down to 43K", ECS Trans., 3 (7), pp. 927-936, 2006.
- [16] K. Petrosyants, O. Dvornikov, N. Prokopenko, M. Kozhukhov, "Extension of Standard SPICE SiGe HBT Models in the Cryogenic Temperature Range", IEEE Int'l. Workshop THERMINIC, 5p., Amsterdam, 2017.
- [17] L. Luo, Z. Xu, G. Niu, P. Chakraborty, P. Cheng D. Thomas, K. Moen, J. Cressler, M. Mudholkar and A. Mantooth, "Wide temperature range compact modeling of SiGe HBTs for space applications", IEEE 43rd Southeast. Symp. on Syst. Theory, pp. 110-113. 2011.
- [18] Rücker, H. J. Korn, and J. Schmidt. "Operation of SiGe HBTs at cryogenic temperatures", IEEE Bipolar/BiCMOS Circuits and Technology Meeting (BCTM), pp. 17-20. IEEE, 2017.
- [19] D. Davidovitch, H. Ying, J. Dark, B. R. Wier, L. Ge, N. E. Lourenco, A. P. Omprakash, M. Mourigal, and J. D. Cressler. "Tunneling, current gain, and transconductance in silicon-germanium heterojunction bipolar transistors operating at millikelvin temperatures", Phys. Rev. Appl. 8, no. 2, pp. 024015, 2017.
- [20] H. Ying, J. Dark, A. Omprakash, B. Wier, L. Ge, U. Raghunathan, N. Lourenco, Z. Fleetwood, M. Mourigal, D. Davidovic, J. Cressler, "Collector transport in SiGe HBTs operating at cryogenic temperatures", IEEE Trans. Electron Dev., vol. 65, no. 9, pp. 3697-3703, 2018.
- [21] B. Heinemann, R. Barth, D. Bolze, J. Drews, G. G. Fischer, A. Fox, O. Fursenko, T. Grabolla, U. Haak, D. Knoll, R. Kurps, M. Lisker, S. Marschmeyer, H. Rucker, D. Schmidt, J. Schmidt, M. Schubert, B. Tillack, C. Wipf, D. Wolansky, Y. Yamamoto, "SiGe HBT Technology with f_T/f_{max} of 300 GHz/500 GHz and 2.0 ps CML Gate Delay", IEEE IEDM Techn. Dig., pp. 688-691, 2010.
- [22] N. Rinaldi and M. Schröter (eds.), Silicon-Germanium Heterojunction Bipolar Transistors for Mm-wave Systems Technology, Modeling and Circuit Applications, River Publishing, The Netherlands, 2018.
- [23] M. Schröter, T. Rosenbaum, P. Chevalier, B. Heinemann, S. Voinigescu, E. Preisler, J.Böck, A. Mukherjee, "SiGe HBT technology: Future trends and TCAD based roadmap", Proc. of the IEEE, vol. 105, no. 6, pp. 1068-1086, 2017.
- [24] D. Miller, Quantum mechanics for scientists and engineers, Cambridge, 2009.
- [25] M. Schröter and A. Chakravorty, *Compact hierarchical modeling of bipolar transistors with HICUM*, World Scientific, Singapore, 2010.
- [26] S. Lin and C. Salama, "A $V_{BE}(T)$ model with application

to bandgap reference design", IEEE J. of Solid-State Circ., vol. 20, pp. 1283-1285, 1985.